Mesh Dependence of Transverse Cracking in Laminated Stainless Steel with both High Strength and High Ductility

Xiang Guo[1, 2], Wenjun Zhang[3], Jian Lu[4,*]

[1] School of Mechanical Engineering, Tianjin University, Tianjin 300072, China
[2] Tianjin Key Laboratory of Nonlinear Dynamics and Chaos Control, Tianjin 300072, China
[3] School of Civil Engineering, Tianjin University, Tianjin 300072, China
[4] Department of Mechanical and Biomedical Engineering, City University of Hong Kong, Hong Kong
* Corresponding author: jianlu@cityu.edu.hk

Abstract A combination of surface mechanical attrition treatment (SMAT) and co-rolling can produce large-scale laminated nanostructured stainless steel (SS) with both high strength and high ductility. Recent numerical results based on the cohesive finite element method have revealed that brittle nanograined interface layer can enhance the ductility of the co-rolled SMATed SS. Here, numerical investigation focuses on effects of both shape of the bilinear cohesive law and mesh size and shows that the larger thickness of the phases in uniform state allows the use of coarser meshes.

Keywords Laminated nanostructured metals, cohesive finite element method, bilinear cohesive law, mesh dependence

1. Introduction

Surface mechanical attrition treatment (SMAT) and co-rolling can be combined to produce large-scale laminated nanostructured metals with both high strength and high ductility [1]. Therefore, it is believed to have a good future to be applied in structural engineering. Through the SMAT, a nano-crystalline surface can be generated for various metals to enhance their yield stress and fatigue life. The co-rolled SMATed metals with nanograined interface layers (NGILs) can be produced. This approach can generate laminated nanostructured 304 stainless steel (SS) with tensile yield stress 878 MPa and failure strain 48% [1].

A computational framework for fracture analysis is in need to investigate the toughening mechanism. The main concern is on the nucleation and the propagation of non-localized microcracks into coarse-grained layer (CGL). Therefore, the cohesive finite element method (CFEM) is appealing to investigate the cracking. The CFEM can model damage initiation/evolution and fracture processes explicitly and has been used to investigate brittle and ductile fracture extensively. The intrinsic CFEM embeds cohesive elements along boundaries of all volumetric elements as part of the physical model [2]. It was adopted in our former studies [3,4]. Our studies have shown that both the critical energy release rate and the thickness of the NGIL play critical roles in determining the overall ductility of the co-rolled SMATed 304SS. However, the dependences of the results on both shape of the cohesive law and the mesh have not been addressed.

2. Mesh dependence issue and numerical framework

Many cohesive laws have been developed [5]. The bilinear cohesive law was used in [3,4], as shown in Fig. 1. $T_{\max}$, cohesive strength, is the stress at which the damage initiates and the

separation is δ_m^0. G_{coh}, critical energy release rate, is given by $G_{\text{coh}} = \int_0^{\delta_m^f} T(\delta)\,\mathrm{d}\delta = 0.5 T_{\max} \delta_m^f$, where T is an effective traction, δ an effective separation, and δ_m^f a critical crack opening. The damage associated with the cohesive surface separation can be defined [6]. Many researchers assumed that $T_{\max}$ and G_{coh} played key roles while the shape of the cohesive law was relatively unimportant. Series of studies indicated that it could lead to unreasonable results [5,7]. Therefore, the shape of the cohesive law should be considered. Dependence of the results on the shape of the cohesive law is closely relevant to the dependence of the results on the mesh. Stress distribution in the cohesive zones must be resolved accurately. Therefore, a minimum number of elements are needed in each cohesive zone and the minimum number has attracted much attention [8]. On the other hand, insertion of cohesive elements introduces fictitious compliance [9]. To alleviate it, Geubelle and Baylor [9] used an adjustable initial slope in the bilinear cohesive law.

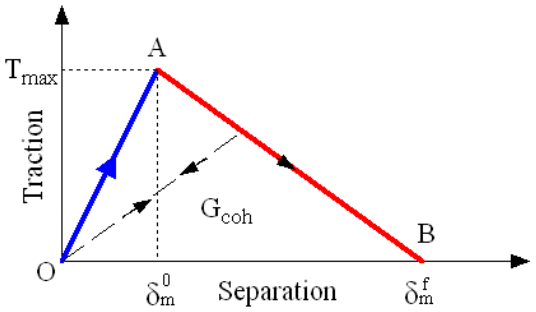

Figure 1. Bilinear cohesive law

The co-rolled SMATed 304SS contains the CGL and the NGIL. A computational configuration with a length 1 mm and a width 0.9 mm is illustrated in Fig. 2. The thickness of the NGIL is taken as 40 μm. Two levels of structured cross-triangular mesh size, namely, 10 by 10 μm and 5 by 5 μm, are used. The cross-triangular meshes with uniform size 10 by 10 μm are illustrated in Fig. 2.

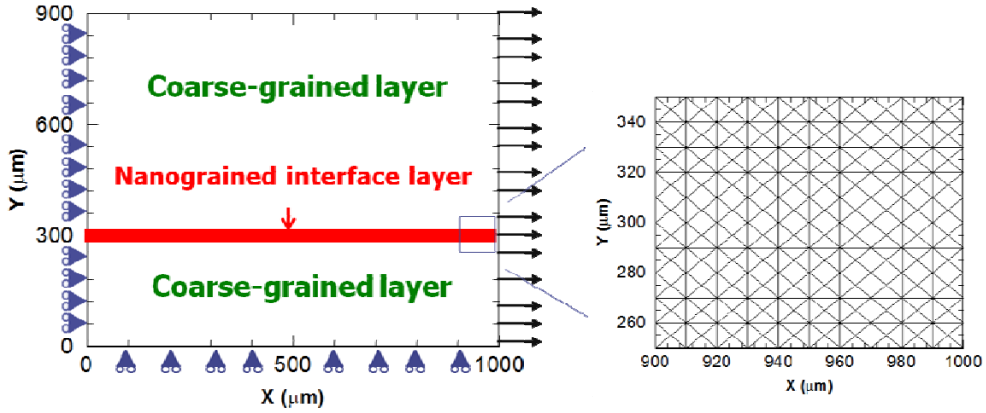

Figure 2. Computational configuration and cross-triangular meshes

Constitutive parameters for the bulk and cohesive elements are listed in Table 1. Both phases are treated as isotropic, elasto-plastic metals. The density, Young's modulus *E*, Poisson's ratio ν, and flow stress for the two phases are the same as those in [3,4]. The critical energy release rate of the CGL, G_{Ic}, is obtained in terms of its fracture toughness K_{Ic}, which is taken as 100 $\mathrm{MPa}\sqrt{\mathrm{m}}$. The cohesive strength of the NGIL can be calibrated at different critical energy release rate and failure strain [3,4]. Two types of boundaries between the CGL and the NGIL are considered: i) a tough boundary implying that its cohesive parameters are the same as those of the CGL and ii) a brittle boundary implying that its cohesive parameters are the same as those of the NGIL. NGIL's failure strain was estimated to be 3.26% [3]. Here, the critical energy release rate of the NGIL is taken as 60 Jm^{-2} and its cohesive strength is calibrated as 1.89 GPa [3,4]. With the calibrated results, simulations are carried out at two levels of the cohesive strength of the CGL ($T_{\mathrm{m}}=1.87\sigma_0$ and $1.94\sigma_0$) and for two types of boundaries.

Table 1. Constitutive parameters for bulk and cohesive elements of the co-rolled SMATed 304SS

Phase	Density $(\mathrm{kg/m^3})$	Yield stress	E (GPa)	ν	$T_{\max}$	G_{coh}
CGL	8000	σ_0	200	0.29	T_{m}	G_{Ic}
NGIL	8000	σ_0'	200	0.29	T_{m}'	G_{Ic}'

3. Numerical results

3.1 Effect of the shape of bilinear cohesive law

δ_m^0 is taken as 10^{-2} μm and 10^{-3} μm. When the mesh size is taken as 10 and 5 μm, the simulated results for the co-rolled SMATed 304SS are shown in Figs. 3(a-b) and 4(a-b), respectively. With δ_m^0 decreasing, the computational burden increases obviously, consistent with the finding in [10], and the overall fluctuation in the stress-strain curve also decreases. As δ_m^0 decreases, simulations show that the peak stress around the microcrack nucleation decreases in Figs. 5 and 6, which is in agreement with [7].

3.2 Effect of the mesh size

For refined mesh, the incipient microcrack occurs relatively earlier, more minor branches occur and then arrest after running one or a few elements length, similar with the experimental study [11]. On comparing Figs. 3 with 4, it can be observed that the stress history when the mesh size is 5 μm is more detailed than that when the mesh size is 10 μm. Meanwhile, at each level of δ_m^0, both the

peak stress before the microcrack nucleation and that after the microcrack nucleation have negligible dependence on the mesh size.

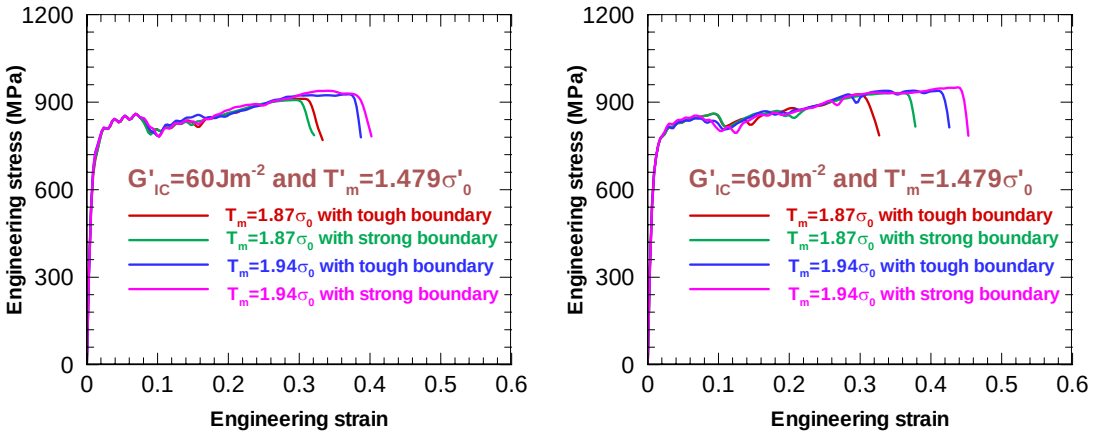

Figure 3. The results with mesh size 10 μm when δ_m^0 is (a) 10^{-2} and (b) 10^{-3} μm

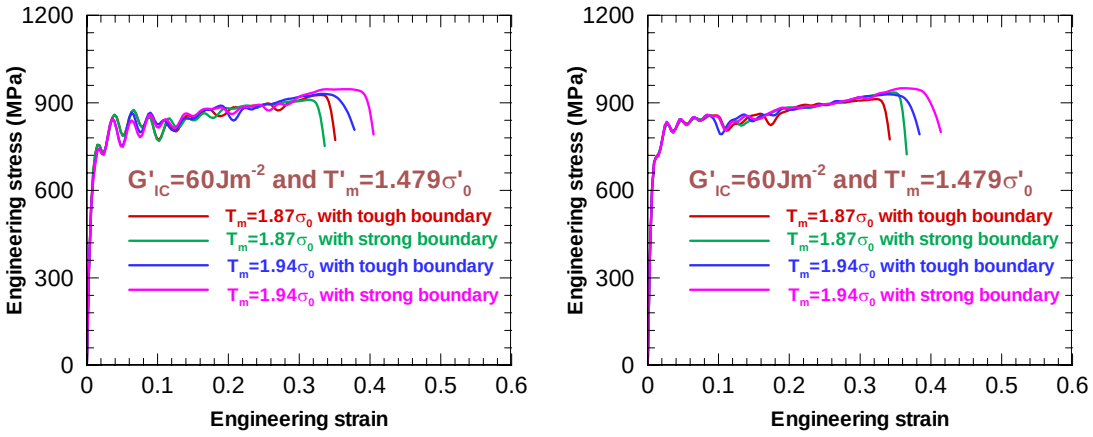

Figure 4. The results with mesh size 5 μm when δ_m^0 is (a) 10^{-2} and (b) 10^{-3} μm

The cohesive zone size has been studied extensively. The widely-used estimate in plane strain condition is Rice's model [12], which gives the cohesive zone size to be $\frac{9\pi}{32}\left(\frac{E'\Gamma_0}{T_{max}}\right)^2$. For the CGL, the estimated cohesive zone sizes are 7690 and 7190 μm. The mesh sizes, 10 and 5 μm, are much smaller than them. For the NGIL, the estimated cohesive zone size is 3.24 μm, smaller than the mesh sizes. Due to its brittle nature, the size of cohesive zones in the NGILs is relatively easy to reach the level of the NGIL thickness. The cohesive zones in the NGILs contain 4 and 8 cohesive elements when the mesh size is 10 and 5 μm, respectively. Therefore, there is no need to further refine the mesh in the NGILs. The above justifies using two levels of mesh size. Note that in Figs. 3 and 4, at each level of δ_m^0, the main results are fairly consistent despite the fact that the mesh sizes are not apparently smaller than the estimated cohesive zone size for the NGILs. Previous

investigation has also suggested that the mesh size requirement can be relaxed under certain conditions [8,9]. Our simulation shows that the larger thickness of the brittle phase in uniform state allows the use of coarser meshes.

4. Conclusions

The simulations show that the shape of the bilinear cohesive law can obviously change the stress response, including the overall numerical fluctuation and peak stress. For crack initiation and propagation in a laminated composite structure, overall stress response has weak dependence on the mesh size. Simulation results show that the comparatively larger thickness of the phases in uniform state relaxes the requirement on the mesh size.

Acknowledgements

Dr. X. Guo acknowledges the support from National Natural Science Foundation of China (Project No. 11102128). Professor J. Lu acknowledges the support from the Research Grants Council of the Hong Kong Special Administrative Region of China under grants CityU8/CRF/08 and GRF/CityU519110, and the Croucher Foundation under grant CityU9500006.

References

[1] A.Y. Chen, D.F. Li, J.B. Zhang, H.W. Song, J. Lu, Make nanostructured metal exceptionally tough by introducing non-localized fracture behaviors. Scripta Mater, 59 (2008) 579–582.

[2] A. Needleman, A continuum model for void nucleation by inclusion debonding. ASME J Appl Mech, 54 (1987) 525–531.

[3] X. Guo, A. Y.T. Leung, A.Y. Chen, H. H. Ruan, J. Lu, Investigation of non-local cracking in layered stainless steel with nanostructured interface. Scripta Mater, 63 (2010) 403–406.

[4] X. Guo, G.J. Weng, A.K. Soh, Ductility enhancement of layered stainless steel with nanograined interface layers. Comp Mater Sci, 55 (2012) 350–355.

[5] N. Chandra, H. Li, C. Shet, H. Ghonem, Some issues in the application of cohesive zone models for metal-ceramic interfaces. Int J Solids Struct, 39 (2002) 2827–2855.

[6] ABAQUS, ABAQUS theory manual and user's manual, version 6.10, Dassault (2012).

[7] H. Li, N. Chandra, Analysis of crack growth and crack-tip plasticity in ductile materials using cohesive zone models, Int J Plast 19 (2003) 849–882.

[8] Z. Zhang, G.H. Paulino, Cohesive zone modeling of dynamic failure in homogeneous and functionally graded materials. Int J Plast, 21 (2005) 1195–1254.

[9] P.H. Geubelle, J.S. Baylor, Impact-induced delamination of composites: a 2D simulation. Compos Part B, 29 (1998) 589–602.

[10] D.V. Kubair, P.H. Geubelle, Comparative analysis of extrinsic and intrinsic cohesive models of dynamic fracture. Int J Solids Struct, 40 (2003) 3853–3868.

[11] E. Sharon, J. Fineberg, Microbranching instability and the dynamic fracture of brittle materials. Phys Rev B, 54 (1996) 7128–7139.

[12] J.R. Rice, The mechanics of earthquake rupture. Physics of the Earth's interior. Italian Physical Society, Italy, North-Holland Publ. Co.: Amsterdam (1980) 555–649.